


Empirical seismic vulnerability, deterministic risk and monetary loss assessment in Fira (Santorini, Greece)

D. Kazantzidou-Firtinidou¹ · I. Kassaras¹  · A. Ganas²

Received: 22 December 2017 / Accepted: 8 May 2018
© Springer Science+Business Media B.V., part of Springer Nature 2018

Abstract A deterministic seismic risk and monetary loss model is presented for the capital of Santorini volcanic Island, the town of Fira, on a building block scale. A local seismic source of M5.6 inferred from a recent volcano unrest in 2011–2012, detailed seismic vulnerability of 435 buildings and site conditions deduced from free-field ambient noise measurements were combined toward assessing the EMS-98 damage grade and its probability to occur. The seismic scenario yielded no damage or slight damage for 84% of the buildings, 16% of the constructions are expected to present moderate-to-heavy damage, while the economic loss amounts to 4 million euros. Although the model predicts low damage and direct economic loss, interaction with the touristic business activities might produce cascade side effects for the economy of the island and consequently Greece's GDP, an important part of which emanates from Santorini.

Keywords Santorini · EMS-98 · HVSR · Seismic risk · Building typologies · Seismic vulnerability · Monetary loss

1 Introduction

Aiming at supporting the full cycle of the natural and environmental disaster management in Greece, a comprehensive seismic risk model has been developed for the town of Fira. Fira is the capital of Santorini Island, one of the most popular destinations for visitors

✉ I. Kassaras
kassaras@geol.uoa.gr

D. Kazantzidou-Firtinidou
dkazantzidou@geol.uoa.gr

A. Ganas
aganas@noa.gr

¹ National and Kapodistrian University of Athens, 15784 Athens, Greece

² National Observatory of Athens, 11810 Athens, Greece

globally. This is due to an outstanding caldera scenery created by intense volcanic phenomena, and in particular by the Plinian volcanic eruption in ~ 1600 BC (Druitt et al. 1999) which in combination with a 9-m tsunami runs up at the Cretan coasts (e.g., Nomikou et al. 2016) destroyed the Minoan civilization and terminated the copper era in ancient Greece. The caldera is presently a rectangular lagoon, approximately 12×7 km² with a depth reaching 392 m, surrounded by a 300-m high steep relief, atop of which the town of Fira is situated.

Apart from the magnificent scenery, Santorini exhibits an urban environment with unique vernacular architecture, found in particular in the towns of Fira and Oia (Bozineki-Didoni 1999). Apart from their cultural–architectural particularity, surprising is the arrangement of terraced buildings, forming a colorful puzzle of “eagle-nests” resting upon the tips of the caldera, a unique spectacular worldwide and the island’s great attraction. Apparently, given the high hazard of the area due to its volcanic and seismotectonic environment, these traditional constructions emerge an increased interest on their seismic response, which has not been yet investigated.

Thanks to the abovementioned and also several other local attractions, Santorini gained a high touristic popularity that culminates during the summertime, with several hundreds of thousands visitors. As a consequence, extensive touristic business located on the island largely contributes to the Greek GDP; hence, its interruption in case of a crisis due to the region’s high natural hazard should significantly impact the country’s economy.

Although volcanism is the major hazard for Santorini, the risk for a disaster by a major explosive event is more manageable, considering that such episodes are rare and moreover, they can be forecasted by the pre-eruptive activity that provides warnings which allow for taking over predetermined plans of evacuation and sheltering actions (e.g., Newhall 2000). It is worth noting that tephra fallout (e.g., Biass et al. 2016a), and/or volcanic ballistic projectiles (e.g., Biass et al. 2016b) which can be produced from a mild volcanic unrest that occurs more frequently, consists of potential hazards for the island, as it may impact its structures. Without underestimating the above hazards and their potential monetary loss for the local society, emphasis herein is given on seismic phenomena that have strongly impacted Santorini in the past (e.g., the 1956 catastrophic event, Papadopoulos and Pavlides 1992).

In January 2011, the volcano reawakened with intense seismic activity beneath the caldera and surface deformation was interpreted by the inflation of a magmatic source (Newman et al. 2012; Papoutsis et al. 2013). The possibility that the magmatic inflation might have increased the seismic hazard of Santorini has motivated this study. Another reason that motivated our effort is the need for coping with adverse circumstances in case of a crisis, given the particularly dense/narrow urban tissue and overcrowding of Santorini during the high season. The importance of a tailored seismic risk mitigation plan for the island is highlighted, contributing to the enhancement of protection and resilience of this region of high cultural, architectural, economic interest and seasonally dense multinational population. To this aim, given that no known relative work has been conducted to date, the seismic hazard, vulnerability of the building stock and the seismic risk of Fira are investigated.

The urban area under study is the central part of Fira. The data used were obtained during an in situ survey conducted by our working group for collecting microtremor recordings and the inventory of the existing building stock. In addition, the footprints of the buildings mapped by SERTIT (Service Régional de Traitement d’Image et de Télédétection, Strasbourg) through satellite images have been used after in situ validation and in juxtaposition with the urban plan. Geological, geotechnical and seismological information available from previous research has also been implemented.

In the next sections, we describe a deterministic seismic hazard model and an empirical vulnerability model for the town of Fira. These two models were combined using semiempirical vulnerability functions, as incorporated into a LM1 macroseismic scheme, developed in the framework of the Risk-UE Programme (Milutinovic and Trendafiloski 2003). This procedure yielded a physical seismic risk and monetary loss model for a M5.6 earthquake scenario on a NE-SW fault in the vicinity of the target site, inferred by the recent 2011–2012 seismic swarm activity (Papadimitriou et al. 2015). The flowchart of Fig. 1 presents the organization of this work. In conclusion, reference is made to the need of a future study focused on the touristic industry and the impact that a seismic crisis may have on it.

2 The seismic hazard model

Santorini is located within the Aegean microplate, which undergoes rapid deformation, related to its convergence with the African continent and the active subduction of the remnants of the oceanic Tethys lithosphere beneath it; as a result, the occurrence of volcanic episodes and earthquakes is common phenomena, which have formed the present South Aegean Active Volcanic Arc (SAAVA) (e.g., Papazachos and Cominakis 1971), part of which is Santorini (Fig. 2a). Among the volcanic centers of the SAAVA, only

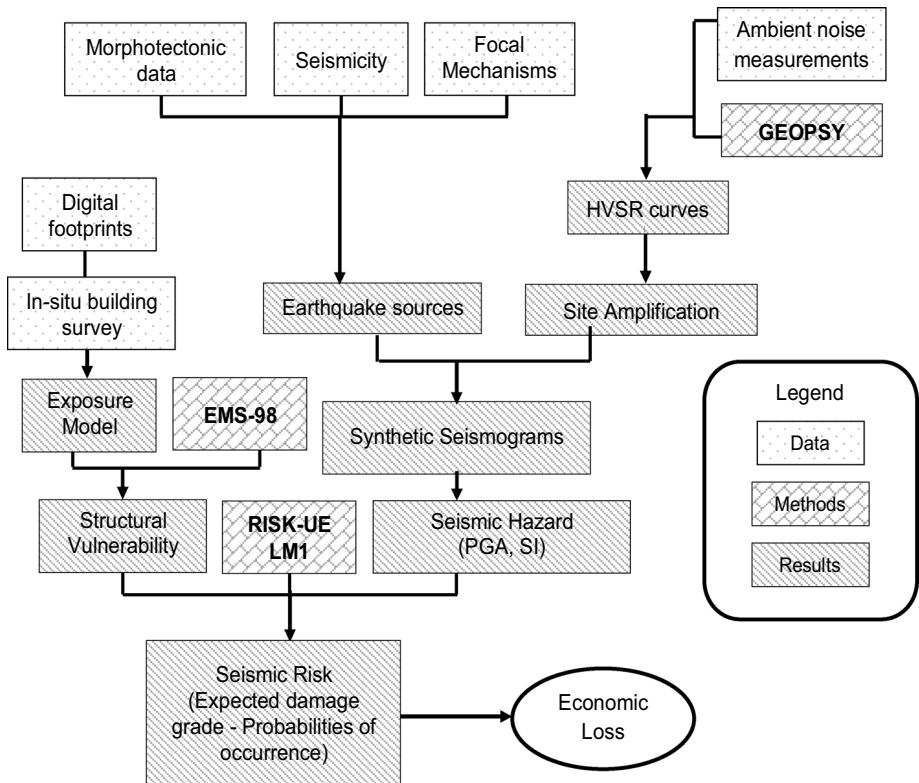
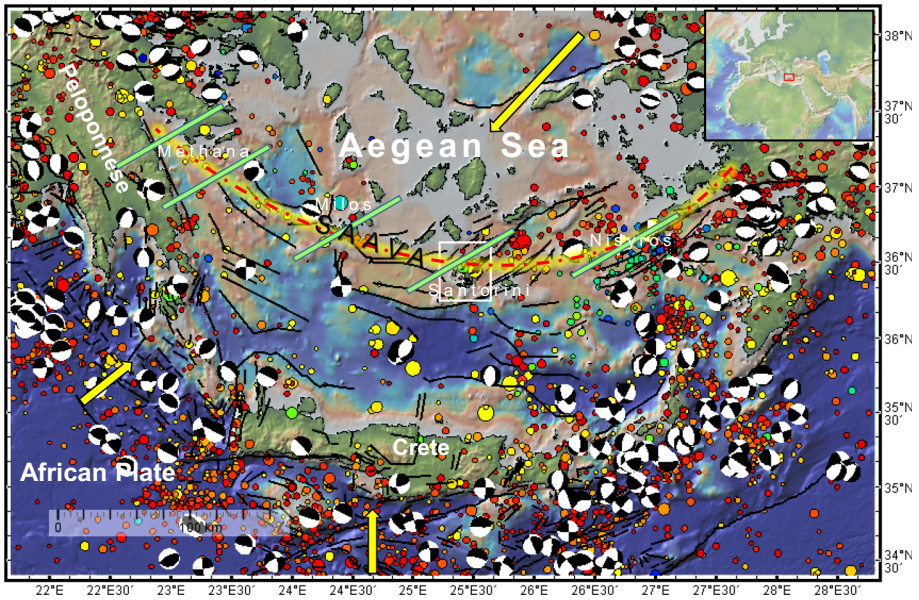
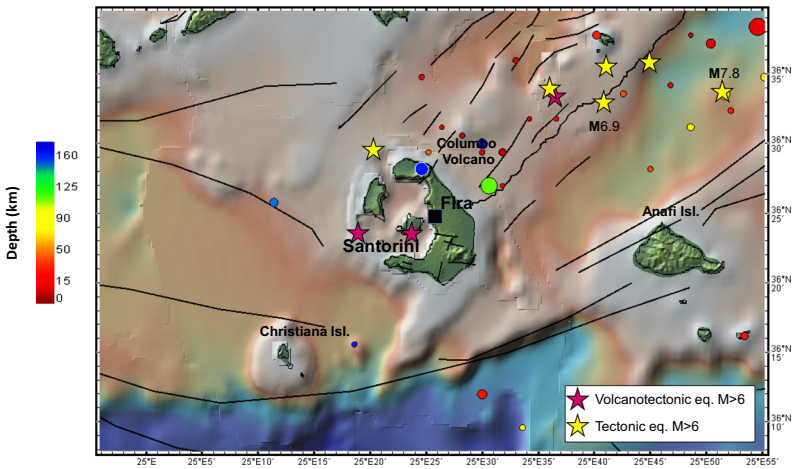


Fig. 1 Methodology and workflow



(a)



(b)

Fig. 2 Top: Seismotectonic map of the South Aegean. Bathymetry and topography are from GeomapApp database. Black lines are main faults (Ganas et al. 2013). Beachballs are GCMT solutions. Earthquake epicenters (solid circles) are from the SHEEC database (e.g., Grünthal et al. 2013). The white rectangle surrounds the Santorini Volcanic Center (SVC). Yellow arrows indicate the direction and the relative amplitude of the plates' motion (Kahle et al. 1998). Greenish bars indicate the direction of active crustal faulting along SAAVA (Papazachos and Panagiotopoulos 1993). Bottom: Map of Santorini (the area of the white rectangle in the top panel). Magenta stars indicate earthquakes prior to 1900 (Papazachos and Papazachou 2003) and yellow stars earthquakes after 1900 (Makropoulos et al. 2012) with $M \geq 6$

Santorini and Nisyros have either erupted or shown significant evidence of unrest during the past 100 years. The last eruption of the Santorini volcano occurred in 1950.

The volcanic origin of Santorini is evidenced by its geology; however, the tectonic context of the volcano is poorly documented (Feuillet 2013). Its prominent seismogenic sources are two tectonic lineaments, capable of producing hazardous earthquakes, namely the Columbo (or Colombos) Line (CL) and the Kameni Line (KL) (Fig. 3). Santorini has been proven vulnerable also due to more distant seismogenic sources, belonging to the system of the South Aegean active faults (Nomikou et al. 2017). Specifically, on July 9, 1956, a M7.8 earthquake, been the strongest earthquake of the twentieth century in the Aegean, and a M6.9 aftershock (Fig. 2b) devastated the island (Papazachos and Papazachou 2003). The former event caused a large tsunami due to submarine landslides that largely affected the eastern coast of Santorini, reaching even the shores of Crete and Turkey with significant run-ups (Okal et al. 2009).

Until recently, the Santorini volcano was in a dormant stage, although a continuous hydrothermal activity accompanied by local weak seismic activity (e.g., Kolaitis et al. 2007) indicated an active field. Recently, in 2011, the volcano entered a period of unrest, characterized by the onset of intense intra-caldera swarm-type seismicity, which ended around the end of February 2012 (Chouliaras et al. 2012; Vallianatos et al. 2013; Papadimitriou et al. 2015; Kaviris et al. 2015). Hundreds of well-recorded small earthquakes, consisting the 96% of the activity during the unrest period (Feuillet 2013), indicated the activation of a segment of the Kameni Line (KL) (Papadimitriou et al. 2015) (Fig. 3). Taking into account the distribution of accurately relocated hypocenters (Papadimitriou et al. 2015), the dimensions of the activated seismic source, namely about 8 km length and 6 km width, were applied in Eq. 1 (Wells and Coppersmith 1994) toward determining the fault's magnitude potential (M):

$$M = 3.93 + 1.02 \cdot \log(\text{AS}), \quad (1)$$

where AS is the fault surface. The inferred fault is found capable of producing an earthquake in the vicinity of Fira with M5.6. Although the magnitude of the seismic scenario is moderate, the effects upon a complex built environment in Fira may be adverse. The latter is supported also by the fact that the town's urban facilities become often over-saturated during summertime; thus, human safety is additionally jeopardized in case of a seismic event.

2.1 Ambient noise HVSR

Given the lack of local recordings of strong earthquakes, stochastic ground motion simulation was performed for the M5.6 earthquake scenario on the KL using the EXSIM (EXtended source SIMulation) code (Boore 2009). The method combines energy radiation from a specific fault source with propagation laws and site amplification for producing seismic motions at specified locations. A tailored urban scale seismic risk model, such as the one presented herein, prerequisites the implementation of site conditions. The latter may significantly vary even in neighboring positions, and thus they play an important role to the earthquake effects by amplifying or de-amplifying seismic excitations at certain frequencies (e.g., Kassaras et al. 2015). Hereby, site conditions were approximated by the horizontal-to-vertical spectral ratios (HVSRs) from free-field ambient noise measurements, following the popular method of Nakamura (Nakamura 1989).

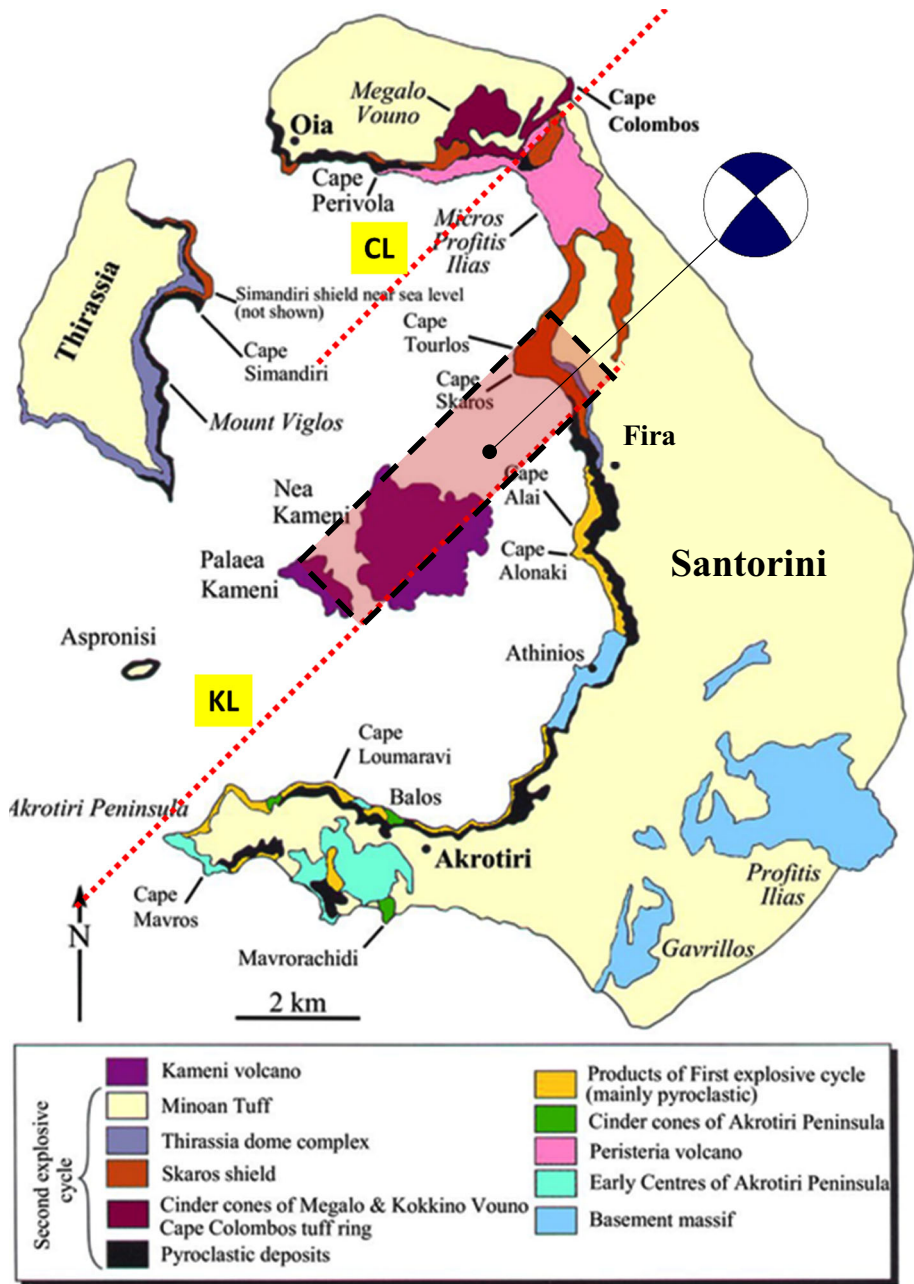


Fig. 3 Simplified geological map of the Santorini complex presenting main volcanic formations and active tectonic features. The pink rectangle shows the surface projection of the KL fault segment for which the earthquake scenario has been developed, while the beachball indicates the average focal mechanism (after Papadimitriou et al. 2015). KL: Kameni Line, CL: Colombo Line. Modified after Petersen (2004)

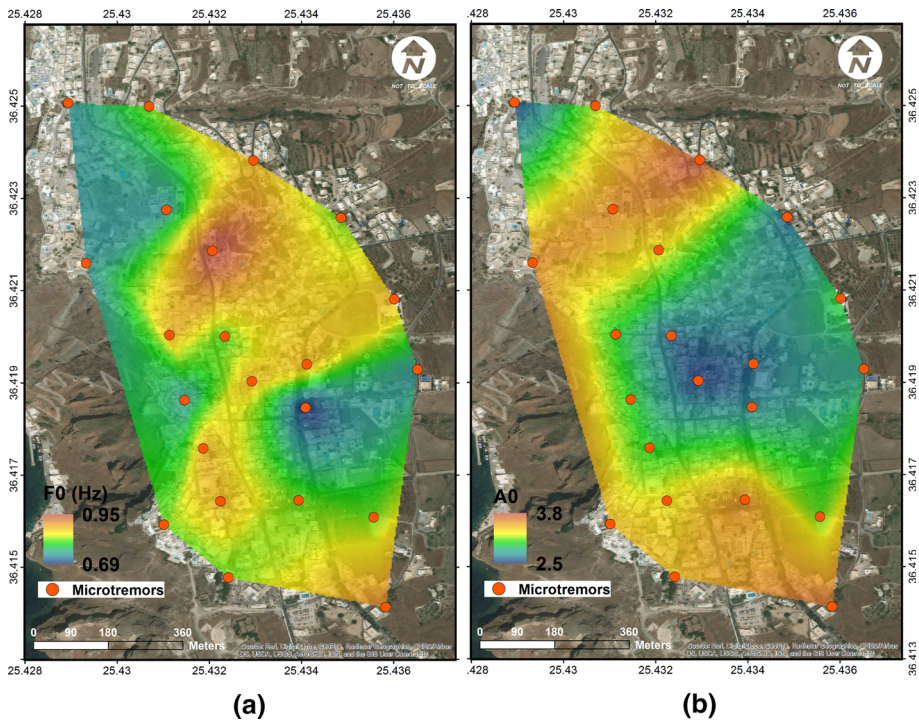


Fig. 4 **a** Fundamental frequency (F_0) and **b** site amplification (A_0) at 21 ambient noise measurement positions in Fira (red solid circles)

Ambient noise records were obtained during December 19–21, 2015 in the municipality of Fira, at 23 locations (Fig. 4). The selection of measurement points was based on their accessibility and the absence of artificial noise sources. All measurements were carried out during daytime. Three-channel REFTEK-130 seismic recorders were used, equipped with Guralp-CMG40T seismometers. The duration of each measurement was 30 min.

HVSR curves were computed using the Geopsy software (SESAME 2005). Geopsy, a suite of software applications for ambient vibration techniques, allows for the implementation of several processing modules (e.g., filtering, smoothing, window selection) enabling quick visualization of the results. The fast Fourier transform (FFT) was calculated for each component and average HVSRs were obtained, further simplified by the use of a Kohno and Ohmachi (1998) logarithmic windowing filter.

After removing two recordings of poor quality due to instruments' malfunction, the dominant (peak) frequency and its corresponding quasi-amplification factor were picked from 21 simplified HVSR curves. These peaks are distributed in the low-frequency range (< 1 Hz) (Fig. 4a). Given the stiff volcanic formations of the study area, one should expect no, or low amplification. However, this is not the case, since amplification ratios are found to be significant, exceeding the value of 2 for all the measurement points (Fig. 4b). We could presume, thus, that the sovereignty of horizontal motion could be related to the steep cliff of the Santorini caldera imposing topographic effects at low frequencies. This effect is particularly evident at the western part of the town, near the tip of the caldera, where higher amplification is observed (Fig. 4b).

2.2 Stochastic ground motion simulation

For the ground motions simulation in Fira, we applied the stochastic finite fault model approach proposed by Beresnev and Atkinson (1998), implemented by Boore (2009) in the EXSIM algorithm that was used herein. The rectangular fault plane of the M5.6 earthquake scenario was divided into smaller subfaults, each of which was then considered to be a point source with a ω -squared high-frequency cutoff spectrum, representing its seismic energy radiation (Brune 1970; Boore 1983). In an iterative procedure including 30 iterations, the hypocenter was placed randomly at one of the subfaults and the rupture was propagated radially with a constant rupture velocity until every subfault was activated. The acceleration spectrum for each subfault $R(f)$ was provided as a result of the convolution of the source, path and site (Joyner and Boore 1988):

$$R(f) = C \cdot S(f) \cdot A(f) \cdot D(f) \cdot I(f) \quad (2)$$

where C is a scale factor, $S(f)$ the source spectrum, $A(f)$ the site amplification factor, $D(f)$ the source-site attenuation function and $I(f)$ a function that controls the instrumental response and filters used in the process. The parameterization of the stochastic model is outlined below:

- The dimensions (8 km \times 6 km) and the magnitude potential (M5.6) of the seismogenic source were considered according to the seismotectonic analyses of Papadimitriou et al. (2015) and scaling laws from Wells and Coppersmith (1994), respectively.
- The fault was divided into six subfaults.
- The stress parameter ($\Delta\sigma$) that controls the shape of the source spectrum $S(f)$ was considered 55 bars as suggested by Margaris and Boore (1998) for earthquakes in Greece.
- The site attenuation parameter κ_0 that controls the high frequencies of the damping function $D(f)$ was considered 0.035, on the basis of a combination of results for the Greek area (Margaris and Boore 1998; Ktenidou et al. 2015).
- The function of the inelastic attenuation $Q(f)$ in use, although negligible in the near field, was the one proposed by Hatzidimitriou et al. (1993) derived from acceleration records in Greece.
- The effect of soil conditions $A(f)$ was approximated by the HVSR curves calculated from ambient noise recordings.

Synthetic Seismic Intensity (SI) was then derived from the simulated horizontal peak ground acceleration (PGA) using the empirical relationship of Tselentis and Danciu (2008):

$$SI(\text{MMI}) = 3.563 \cdot \log(\text{PGA}) - 0.946, \quad (3)$$

where MMI is Modified Mercalli Intensity. Equivalence between MMI and EMS-98 scales is recognized (Musson et al. 2010) and thus its implementation was selected for the herein EMS-98 damage grade estimation (Eq. 4). Figure 5 presents the resulted distribution of the simulated PGA and SI, which reach 285 cm/s² and 7.8 at the western “caldera” section of Fira, respectively.

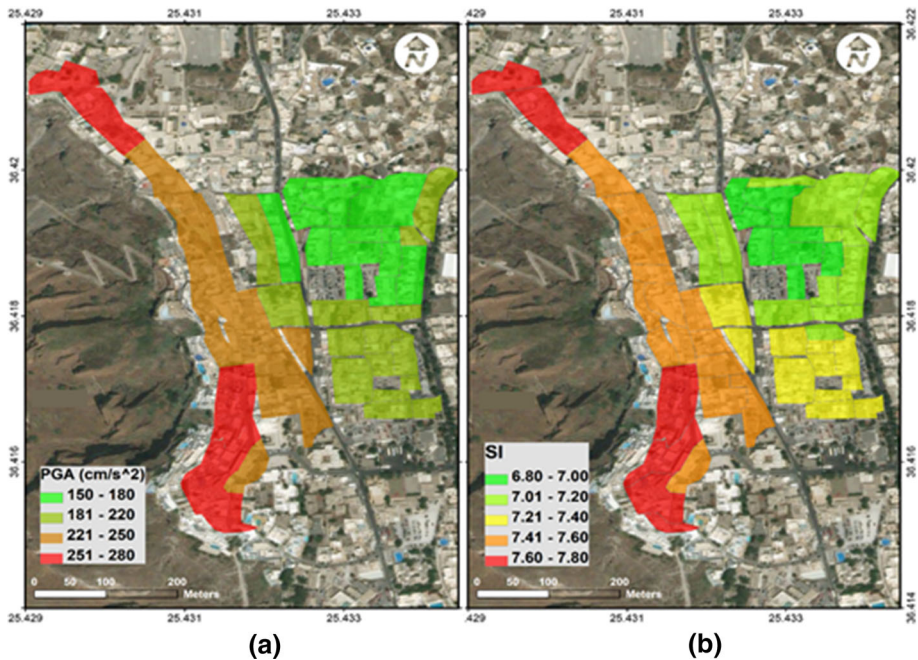


Fig. 5 Synthetic Peak Ground Acceleration (PGA) (a) and Seismic Intensity (SI) (b) in Fira for the M5.6 earthquake scenario

3 The buildings exposure model

The building stock of Fira is very particular, related to the long history of Santorini, the rapid touristic development, and its complex geology and morphology. According to census data (EL.STAT. 2011), 1661 buildings are registered at the municipal community of Fira. Since Santorini is one of the most touristic places in Greece, the registered 1:1 ratio between buildings and permanent residents (1616 people) is largely reduced during the high touristic season. Moreover, the large demand for touristic lodging from mid-1970s led to an uncontrolled construction and expansion of Fira without updating of the urban plan or respect of the structural heritage, the modern urban and safety guidelines. According to Brüstle et al. (2014) after the devastating 1956 earthquake, with an aftermath of 53 deaths, 100 injuries, severe damage to more than 3000 buildings, complete collapse of more than 500 houses and thousands of homeless civilians, construction throughout the island was expanded rapidly so as to satisfy urgent needs for accommodation. Repair and retrofitting works took place at a later time when land values raised.

In this context, new structures were erected at the central and eastern part of the town of Fira. On the other hand, expansion of the town to the north and south has taken place mainly during the last 30 years obeying the huge demands for touristic accommodation. Side effect of the latter was a large amount of arbitrary constructions, leading to distortion of the urban and natural landscape inducing additional vulnerabilities (Beriatos 2008).

The current building stock of the town appears quite complex, consisting of a mixture of vernacular architecture and modern structures, whereas important structural interventions are frequently involved. The herein building exposure model was constructed by an in situ

survey of the urban tissue of the central part of Fira conducted in December 2015. A total of 435 buildings corresponding to 51 building blocks were externally inspected. We notice that buildings of public use, i.e., schools, churches, museums, administration offices, are excluded from this study due to their particular structural design. Five building categories were registered as described in the following subsections.

3.1 Reinforced concrete (RC) buildings with infilled frame lateral resisting system (Fig. 6a)

This typology represents the major population of the town's building stock (82%) (EL.STAT. 2011). After the disastrous earthquake of 1956, reinforced concrete has become the prevailing construction material used for reparation works and new constructions. Moreover, by the mid-1970s, when the touristic exploitation of the island was launched, the main material in use was reinforced concrete, generally preserving the architectural aesthetics.

The main vertical and lateral load bearing system of these buildings is the beam-column frame, occasionally with RC shear walls around the stair case. The frames are infilled with hollow clay or cement brick panels. The floors are full cast, in situ RC slabs of ~ 20 cm thickness, and the roof is either similarly constructed in vaulted configuration, or in bricks. The commercial buildings of the town center typically include a tall soft ground story. According to local engineers' testimony, salty water and sulfurous earth frequently used together with large sea pebbles in the concrete mixture led to non-homogeneous concrete behavior and corrosion of the embedded reinforcement. In addition, improper and often non-engineered practices applied ended up with poor construction detailing.



Fig. 6 **a** RC buildings; **b** simple stone buildings; **c** ground floor in stone and additional floors in RC frame; **d** post-seismic cement brick vaulted structures; **e** mixed buildings with brick-cement vaults at the ground floor and overlying RC frame; **f** excavated dwellings

3.2 Stone buildings, survived from the 1956 earthquake (Fig. 6b)

This type of structure is mainly found at the old town, the “caldera sector.” The bearing walls consist mainly of uncoursed random rubble stone masonry of ultramafic volcanic rocks of high compressive strength. These are disorderly placed in two loosely interlocked wyths in combination with light pumice stone. Pozzolanic mortar with rich hydraulic properties is used in large quantity. Since structural timber was rare and expensive on the dry island, the thick sidewalls were bridged with remarkably thin masonry vaults. Only bourgeoisie houses have flat roofs, often transformed with the addition of parapets. The colors still embedded in the plasters of these older structures are a remembrance of the era prior to the whitewashed facades, imposed as a disinfecting and sun protection measure by the dictatorial regime in the beginning of the twentieth century (Stasinopoulos 2002).

These buildings, in place prior to the disastrous earthquake of 1956, suffered partial or total collapse during the catastrophic event. Some of the surviving ones have been subjected to repair and renovation works and are currently in use. Characteristic is the case of the commercial buildings in the old town where often the stone walls were preserved, even partially, and RC elements have been added in plan, especially in the stores façade. According to local testimonies, proper engineering studies and strengthening works preceding the interventions were rare. Therefore, having no further information regarding the quality and typology of intervention, the stone walls have been considered as the prevailing lateral bearing system in our analysis.

A variation of this typology concerns the buildings of the old town, of which the ground floor, or the partially embedded basement, is stone walls remnants from the 1956 earthquake. On top of the latter, one or more stories of RC frame have been erected, however without clear evidence whether the vertical elements reach the ground to support the new construction, or the original stone walls have been properly confined to accommodate the additional load (Fig. 6c).

3.3 Post-seismic cement brick vaulted buildings (Fig. 6d)

In the aftermath of the disastrous earthquake of 1956, there was an imperative demand of housing of hundreds of people (~ 2000 permanent residents according to Dekavallas 2013). For this purpose, 750 buildings of this type were constructed in newly established settlements across the island and 300 in existing ones, during the so-called aseismic reconstruction of Santorini (Dekavallas 2013). The buildings were provided to the inhabitants whose properties were situated in hazardous zones and the access was restricted, i.e., along the tip of the caldera cliff; in a parenthesis, we mention that these areas are currently structured and populated.

The buildings of this category are one-storey structures (Fig. 7a), able to accommodate one or two families, constructed in the principles of the traditional excavated vaults that are described below. In the absence of transportation facilities after the earthquake, due to the destruction of the main part of the island, local materials were used for the new constructions. Hence, cellular cement–pumice bricks of typical dimensions $20 \times 20 \times 40$ cm (Fig. 7b) were used for the bearing walls and as voussoir stones of the vaults (Fig. 7c). Due to the limited availability of timber to be used as formwork, the “vault” technique, compatible to the traditional one, was adopted. The bricks were put in place with reinforcement bars crossing their section. The vaulted roof and the limited openings, as well as

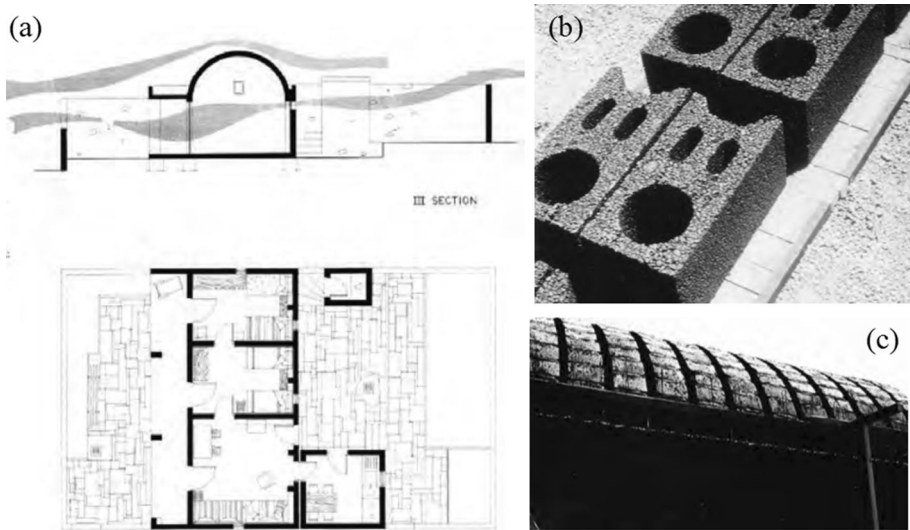


Fig. 7 a Cross section and plan view of a type of aseismic vault; b cement–pumice cellular bricks; c construction of bricked vaults (Dekavallas 2013)

the western orientation of the new structures, constitute one of the first samples of sustainable construction in Greece (Dekavallas 2013).

3.4 Mixed buildings: post-seismic cement brick vaulted structure at the ground floor, RC frame building erected above (Fig. 6e)

This typology is the result of the touristic over-construction of Santorini; one or two stories of infilled RC frame were erected above the existing post-seismic cement brick vaulted buildings described above. The columns of the overlying floors are detached from the ground floor vaulted structure, being directly founded on the ground. In the framework of this study, only the newer upper story has been considered in the vulnerability analysis, assuming that the masonry structure of the ground floor contributes as a rigid infill panel; therefore, a high degree of vertical irregularity was attributed to this typology.

3.5 Excavated dwellings (Fig. 6f)

They are cavernous structures, dug into the Thira pumice slope, occasionally with an additional part lying above the ground. The origin of this vernacular structure dates back to the piracy era, offering the locals a shelter, as well as protection from the wind and the solar heat. These structures are mainly found in the old “caldera sector”; they consist of interconnected stepwise excavated dwellings following the natural inclination of the slope of the caldera (Fig. 8a).

The surface structures of these stepwise terraced caverns are typically made of undressed stone walls (Bozineki-Didoni 1999). These structures are horizontally arranged with their ceiling being the veranda of the overstructures (Fig. 8a), and it is generally difficult to distinguish their limits. Each cavern of these constructions is typically divided into 2–3 rooms, and vertical ducts run through the ground to allow lightning and

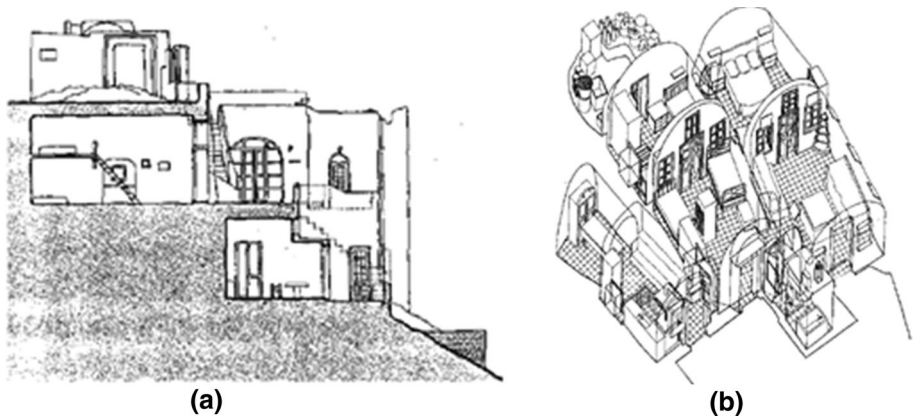


Fig. 8 **a** Cross section of stepwise excavated dwellings; **b** typical interior of excavated houses. From Stasinopoulos (2002)

ventilation (Fig. 8b). A minimum thickness of the perimeter walls guarantees the stability of the overlying cavern(s). Besides the ease of construction of these dwellings and their green architecture, their earthquake performance is outstanding. Following the principles of tunnel constructions (e.g., Wang 1993), the excavated dwellings perform better than surface structures, as they display significantly greater degrees of redundancy thanks to the support from the ground. Indeed, the excavated parts of the Santorini dwellings remained intact after the 1956 event while only their external extensions occasionally collapsed (Dekavallas 2013).

Renovation and construction works, currently pursued in an attempt to preserve the stair-like urban tissue, include inner strengthening of the excavations with steel mesh and shotcrete. However, taking into account that the thickness of the successive tunnel roofs was not conceived to bear multi-story structures, successive excavations along the “caldera” likely reduce the slope stability. For the herein vulnerability analysis, the influence of strengthening has been omitted due to lack of data, while the excavated stories were considered autonomous within the terraced constructions.

Figure 9 summarizes the Fira buildings’ inventory on a building block scale. Figure 9a presents the distribution of buildings as per period of erection and construction material, while Fig. 9b illustrates the buildings type of use. Regarding the construction period, the characterization was decided with respect to the evolution of the Earthquake Resistant Design (ERD) codes in Greece (Table 1). However, in situ identification of the age of buildings was not always a straightforward task; thus, locals’ testimonies, engineering expertise, photographic and other material from the literature were considered in addition.

In summary, the majority of the older structures, as well as the masonry and mixed ones, are concentrated in the “caldera” western sector of the town. Regarding the type of use of the surveyed building stock, 24% are hotels and entertainment buildings, 35% residential, 30% commercial and 6% of mixed use (residential/commercial); these are arranged at distinct sectors of the town (Fig. 9b).

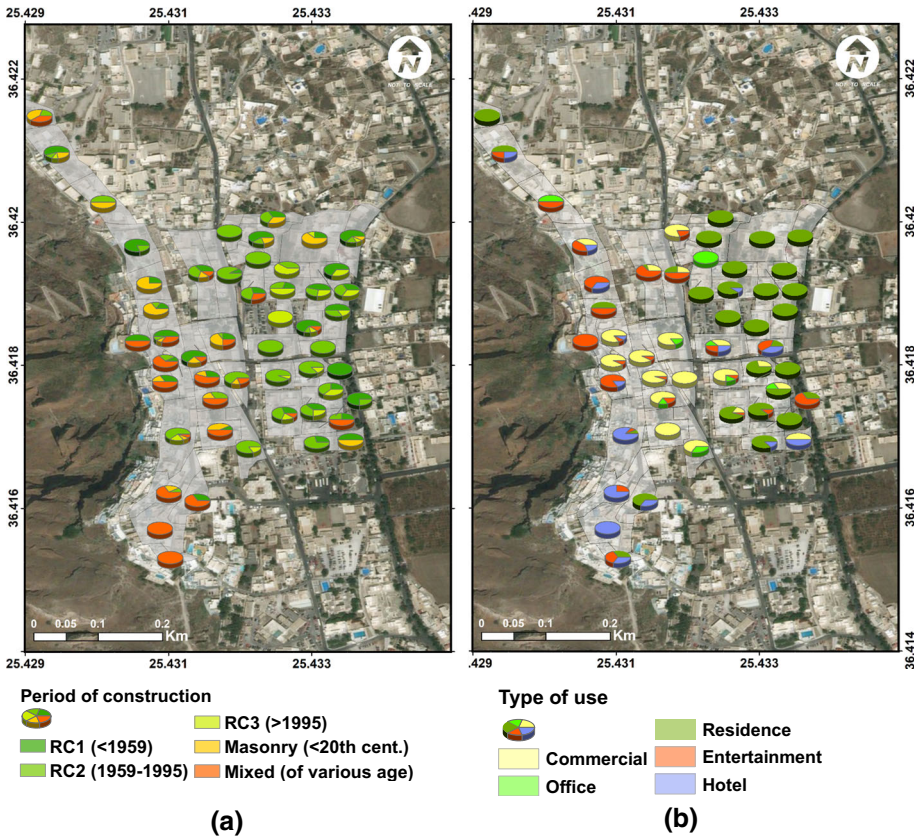


Fig. 9 Distribution of buildings according to **a** the construction period and material and **b** the occupancy type

4 Structural vulnerability assessment

In this section, we describe the vulnerability model of the target site, employing the obtained exposure model. Given the limited data availability regarding the structural characteristics of the exposure model and also the limited resources for an analytical study, the method implemented for the seismic vulnerability is the empirical–macroseismic one, documented as RiskUE-LM1 (Milutinovic and Trendafiloski 2003). The method applies the vulnerability model of EMS-98 (Grünthal 1998) for the typological characterization of the building stock using vulnerability indices within a probability range, adopted by behavior modifiers accounting for the structures’ particularities.

The method was applied by assigning to each building of the derived exposure model one of the existing structural typologies per EMS-98 and a corresponding typological vulnerability index (V_i^*) per Giovinazzi and Lagomarsino (2004) using engineering judgment. The typological V_i^* corresponds to the most probable value, while its uncertainty range is assumed according to Giovinazzi and Lagomarsino (2004) who analyzed a large amount of damage data using the fuzzy sets theory. Thereafter, critical structural characteristics for the buildings’ seismic performance were taken into account by applying

Table 1 Descriptive elements and vulnerability indices and behavior modifiers for existing structural typologies

Descriptive elements	Attributes and vulnerability classes per EMS-98	Vulnerability index (V_i^*) and modifiers per G&L ⁽¹⁾ and this study ⁽²⁾
Number of stories	Low ($n \leq 2$)	- 0.04 ⁽²⁾
	Medium ($n \leq 5$)	0 ⁽²⁾
	High ($n > 5$)	+ 0.04 ⁽²⁾
Lateral load-resisting material and system	Reinforced concrete (RC) cast-in place infilled frame	According to ERD Code
	Post-seismic cement brick vaults: reinforced or confined masonry (M7-vuln. C or D)	$V_i^* = 0.451$
	Masonry simple stone (M3-vuln. B)	$V_i^* = 0.74$
	Mixed buildings: Post-seismic cement brick vaulted structure with RC frame	RC ⁽²⁾ $V_i^* = 0.484$
	Mixed buildings: existing stone walls at the ground floor and RC frame at the first floor or coexistence of stone walls and RC elements	M3 ⁽²⁾ $V_i^* = 0.74$
	Excavated dwellings	External part—M3 ⁽²⁾ $V_i^* = 0.74$
Earthquake Resistant Design (ERD)	Period 1 (< 1959): without ERD code (RC1—vulnerability C)	$V_i^* = 0.644$
	Period 2 (1959–1995): moderate ERD code (RC2—vulnerability. D)	$V_i^* = 0.484$
	Period 3 (> 1995): modern ERD code (RC3—vulnerability E)	$V_i^* = 0.324$
Aggregate building (elevation)	Adjacent buildings with different height	+ 0.02 ⁽²⁾
	With/without staggered floors	+ 0.04 ⁽²⁾
Vertical irregularity	“Soft storey”	+ 0.04 (masonry/RC1) ⁽²⁾ + 0.02 (RC2/RC3) ⁽²⁾
	Change in vertical structure (mixed)	+ 0.04 ⁽²⁾
Aggregate buildings (position)	One side: header	+ 0.06 (stone) ⁽²⁾ + 0.04 (for all RC types) ⁽²⁾
	Two sides: middle	- 0.04 (stone)/0.00 (RC) ⁽²⁾
	Three sides or two sides in perpendicular directions: corner (insufficient aseismic joints)	+ 0.04 (for all RC types) ⁽²⁾
	Detached: isolated	0 ⁽¹⁾
Slope inclination (i)	Flat ($i < 15^\circ$)	0 ⁽¹⁾
	Slope ($i > 15^\circ$)	+ 0.04 ⁽¹⁾
Foundation type	Shallow	0 ⁽¹⁾
	Shallow—different level footings	+ 0.04 ⁽¹⁾
State of preservation	BAD	+ 0.04 ⁽²⁾
	Retrofitted	- 0.08 ⁽²⁾
	Intervention	+ 0.08 ⁽²⁾

G&L: Giovinazzi and Lagomarsino (2004)

behavior modifiers after Giovinazzi and Lagomarsino (2004) and engineering judgement in order to obtain a total vulnerability index per building ($VI = Vi^* + \text{modifier}$).

The herein RiskUE (or EMS-98) taxonomy scheme was based on the material, the structural bearing system and the erection period, as described in Sect. 3. Hence, the stone buildings (Fig. 6b), irrespective of the mechanical characteristics of the construction materials, correspond to the “simple stone” M3 typology, to which the masonry walls, linked with flexible diaphragm, are the bearing elements of both vertical and lateral loading. When stone walls and RC elements were found to coexist in plan, the wall system is assumed to be the prevalent one, with a result to attribute the M3 typology to these mixed buildings. Regarding the post-seismic cement brick vaulted buildings (Fig. 6d), although the steel bars crossing the bricks do not seem to have an active reinforcement role to the lateral response of the walls, expert’s judgment recognizes lower vulnerability to the cement–pumice bricks; thus, M7 “reinforced masonry” typology was assigned. Contrary to the performance of the mixed stone–RC buildings (Fig. 6c), in the case of a double vertical system (vaulted structure with RC frame—Fig. 6e), it was assumed that the wall structure of the ground floor acts as rigid infilling of the frame of the two-story RC structure, with increased vulnerability due to irregularities and intervention.

The distinction of the RC buildings (Fig. 6a) in three categories has been made with respect to the seismic code in force during their erection:

- RC1—Prior to 1959: No Seismic Code.
- RC2—1959–1984: The first official Earthquake Resistant Design (ERD) code with a constant seismic coefficient amplified according to the soil class. According to locals’ experience, the implementation of seismic provisions was limited in Santorini, and it was not earlier than in the 1970s that they were put in force. In 1984, the seismic code was slightly improved by additional articles.
- RC3—1995–today: Dynamic and performance-based design, (NEAK 1994). Introduction of the probabilistic seismic acceleration design spectrum, which replaced the use of the constant seismic coefficient. NEAK (1994) was accompanied by new seismic hazard provisions dividing the country into four zones with significantly increased ground motion coefficients with Santorini belonging in seismic zone II with design $PGA = 0.16\text{ g}$, with 10% probability of exceedance in 50 years. In 2004, the hazard map was updated by the division of the country in three zones, predicting $PGA = 0.24\text{ g}$ for Santorini (EAK 2004).

Table 1 summarizes the descriptive information and the typological classifications together with the modifier scores contributed to the final VI estimates. It is noted that, due to the particularity of the topography and the buildings architecture, additional behavior modifiers were considered, accounting for the regional vulnerability factor suggested by Giovinazzi and Lagomarsino (2004).

The results of the vulnerability analysis are illustrated in Fig. 10. As it can be seen in the pie chart of Fig. 10, the reinforced concrete typologies compose more than half of the building stock of the town, with the 35% corresponding to mid-ERD structures of moderate vulnerability (RC2). The significant multitude of vulnerable masonry old structures (30%) dominates the overall vulnerability scheme of the target site. The spatial distribution of the VI per building block indicates high vulnerability indices in the old “caldera” sector, which includes most of the masonry and mixed buildings.

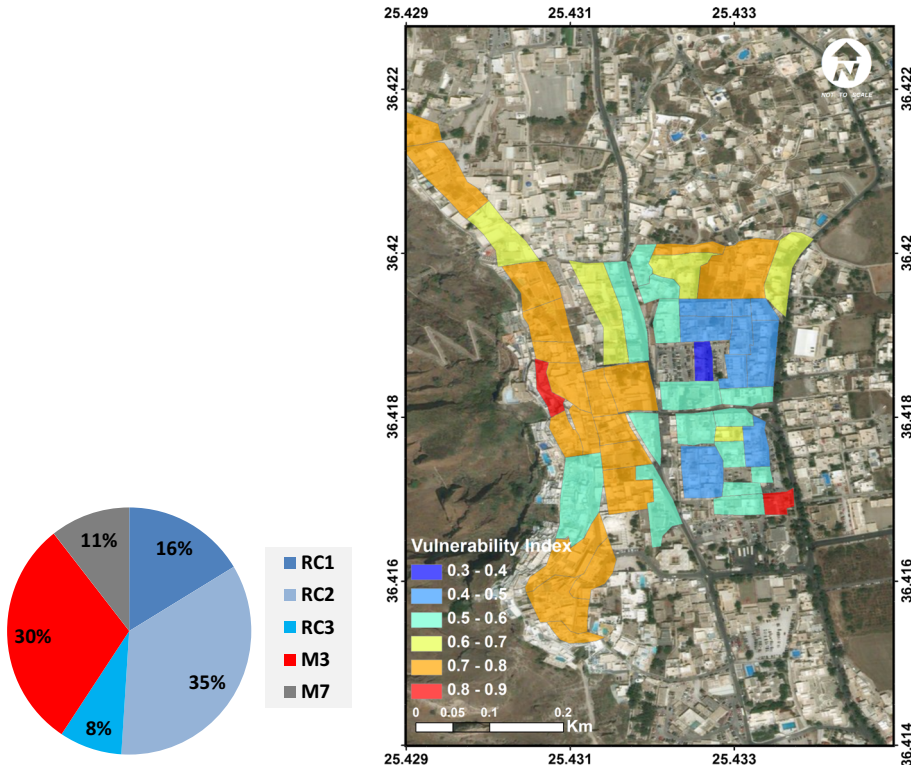


Fig. 10 Left: Pie chart showing the distribution of vulnerability typologies; Right: mean vulnerability index per building block

5 Seismic risk and monetary loss

5.1 Seismic risk

The seismic risk in terms of physical damage of the structures has been evaluated according to the RiskUE-LM1 methodology (Milutinovic and Trendafiloski 2003), which implements the distribution of the mean damage grade (μ_D) per building through the vulnerability index (VI) and the Seismic Intensity (SI), by means of the semiempirical function of the form:

$$\mu_D = 2.5 \cdot [1 + \tanh(SI + 6.25 \cdot VI - 13.1)/2.3)] \quad (4)$$

The probability of reaching or exceeding a certain damage grade (DG) was obtained by the cumulative beta distribution. DG is a discrete value expressed by six variables: D0-No damage, D1-Slight damage, D2-Moderate damage, D3-Substantial to heavy damage, D4-Very heavy damage, D5-Destruction. Herein, only damage due to the ground shaking was taken into account by implementing the derived SIs, neglecting earthquake secondary effects. The most probable vulnerability index (Giovinazzi and Lagomarsino 2004) has been adopted, leading to a deterministic mean DG estimate and its probability per building.

The M5.6 seismic risk scenario was determined in terms of the distribution of the most probable DG per building. Figure 11 presents the most probable DG according to the beta

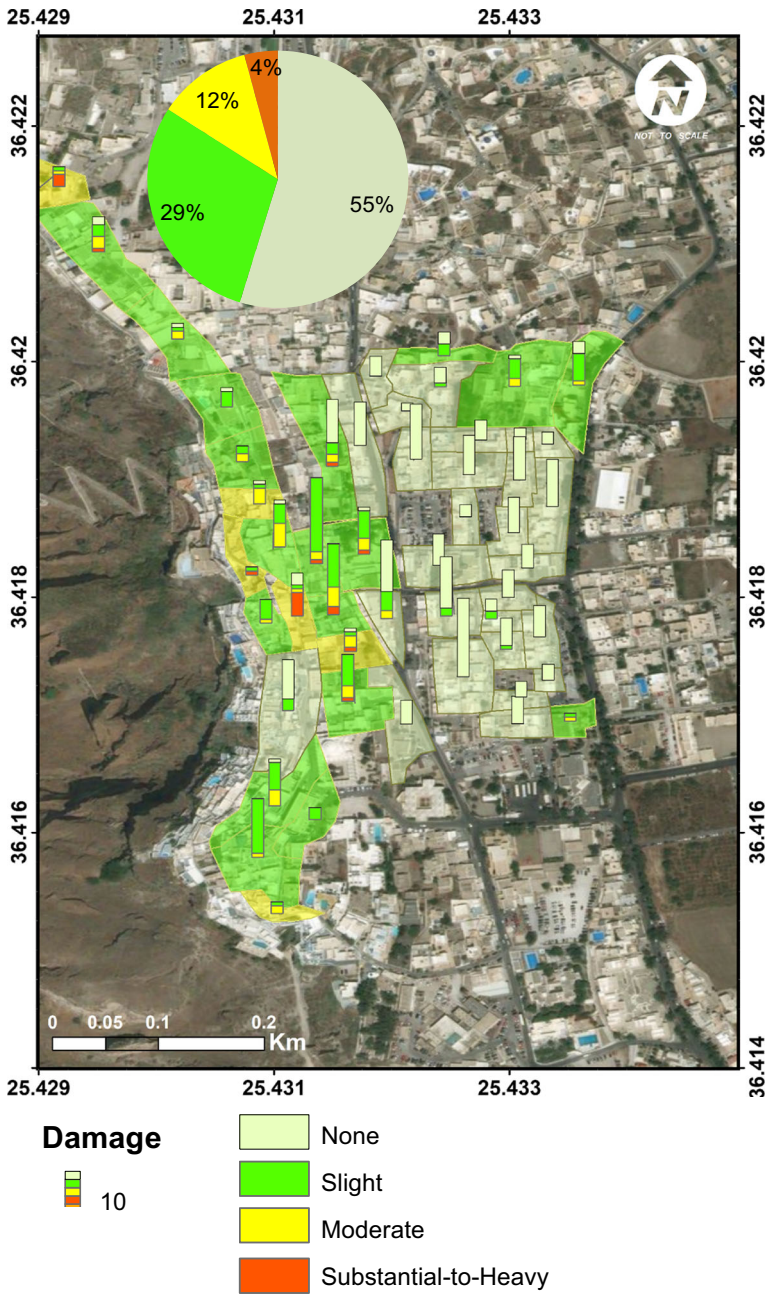


Fig. 11 Most probable mean damage grade per block (polygon areas); number of DGs per building block (stacked bars); overall most probable damage distribution (embedded pie)

distribution of the average μ_D per building and building block. The inset pie summarizes the scenario damage distribution in percentage of the total building stock; the largest amount of the structures is expected to experience no or slight damage (55 and 29%, respectively), while 12 and 4% are expected to experience moderate and substantial-to-heavy damage, respectively.

This qualitative representation of risk is addressed to the civil protection authorities for contingency planning and may also be of use for increasing the public risk perception, motivating prevention and preparedness. Higher damage is expected in the “caldera” sector, while for better apprehension of the estimated risk, the damage grade distribution per building within each block is illustrated (Fig. 11). When focusing on the “caldera” sector, 40 buildings would most likely exhibit moderate and substantial-to-heavy damage. This may be proven particularly adverse for human safety, given the concentration of touristic population in this spot, in combination with the narrow urban tissue.

5.2 Monetary loss

The most comprehensive outcome of the present analysis is expressed in quantitative monetary terms. The expected economic loss is formulated as the accumulated contribution of all DGs into monetary loss, together with their corresponding probability of occurrence, provided the selected seismic hazard model. Although several aspects of the regional—and not only—economy may be affected by such a scenario, only the cost of a new construction, with structural and non-structural elements, has been considered. Content and land cost as well as income-related and indirect loss are out of scope of the present study.

Consequence models or damage ratios are the basic parameters required for loss modeling, connecting damage grades with loss terms. In the current study, given the absence of resources on relevant exposure models, consequence models available in the literature were adopted with targeted modifications after expert’s judgment (Table 2). More specifically, the damage ratios for the most common typologies of reinforced concrete and stone masonry walls were applied as proposed by Kappos et al. (2006) for the Greek built environment. Reference is made also to the work of Goretti and Di Pasquale (2004), which was used for assuming the cement brick damage ratios based on damage ratios of enhanced quality stone walls.

The replacement cost per unit floor area is assumed equal to 900€/m², of which only 30% is supposed to correspond to structural works of the bearing system, according to local engineers estimates. This value is a rough estimate for the cost of structural and non-

Table 2 Damage (loss) ratios per damage grade for RC and masonry structures

Damage grades	Stone (A)	Cement brick (C)	Reinforced concrete
Literature	Kappos et al. (2006)	Modified after Goretti and Di Pasquale (2004)	Kappos et al. (2008)
DG1	2%	2%	0.50%
DG2	12%	10%	5%
DG3	30%	27%	20%
DG4	55%	50%	45%
DG5	85%	80%	80%

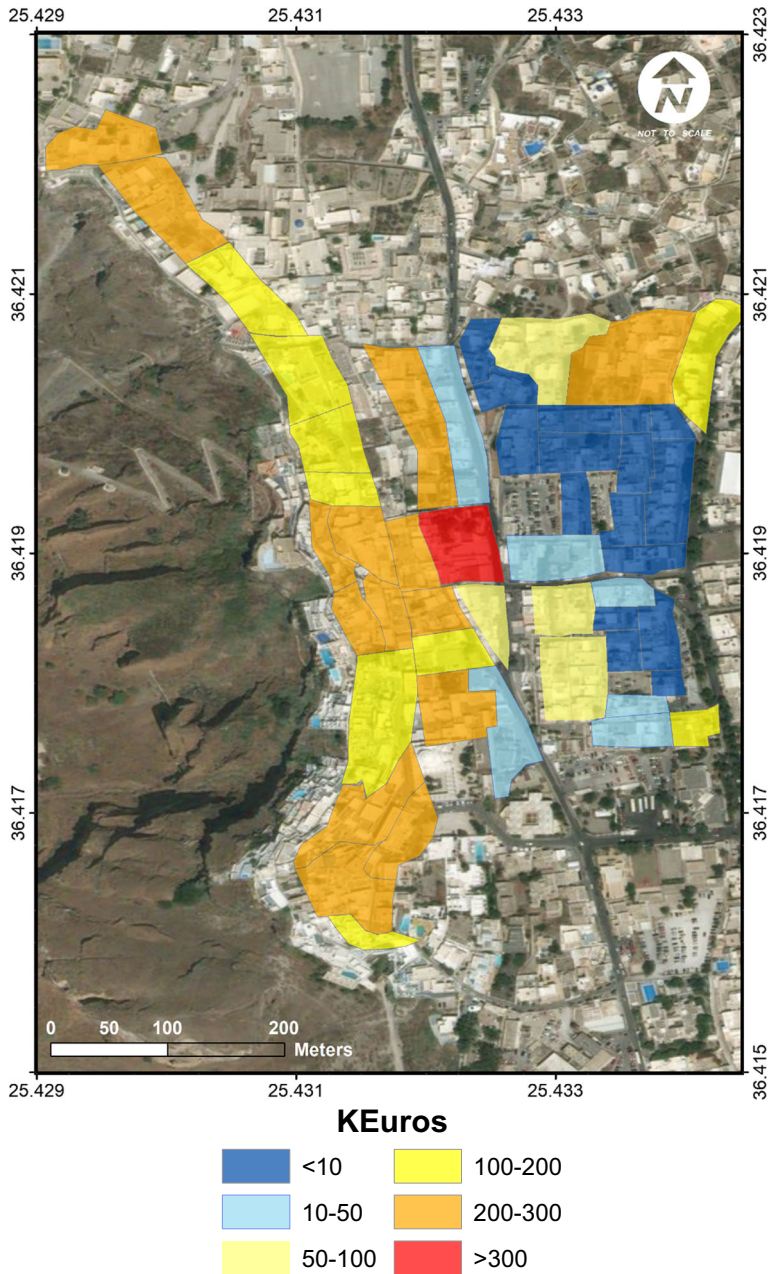


Fig. 12 Estimated economic loss for the M5.6 seismic scenario

structural elements of a medium quality construction in Santorini, taking into account the specificities of the island and the area’s conditions for human labor, material transportation facilities or foundation works. Figure 12 presents the distribution of the estimated loss for

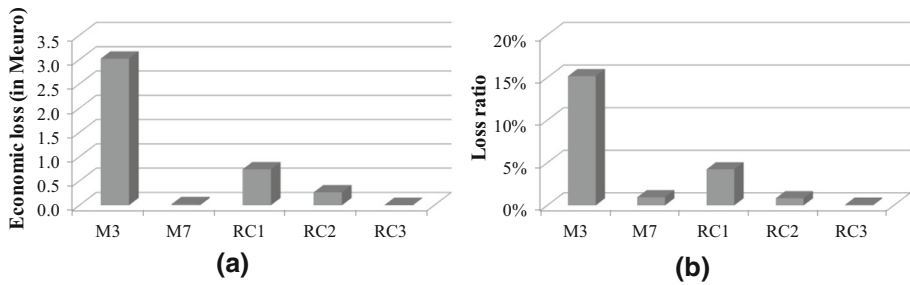


Fig. 13 **a** Total economic loss per structural typology for the seismic scenario studied in MEuro and **b** loss ratio per structural typology

the M5.6 seismic scenario on a building block level. The total economic loss for the given earthquake scenario in the area of study is estimated of the order of 4 million euros.

For better understanding of which building typologies contribute more to the overall economic loss, losses have been aggregated per building typology, as presented in Fig. 13a. It is evident that the majority of the total economic loss is attributed to the stone masonry buildings (M3). This estimate is due to the combination of three factors: the large multitude of this typology (30% of the studied building portfolio), their inherent vulnerability further increased by registered structural irregularities, potential interventions and state of preservation, as well as their spatial correlation with the highest PGA values across the “caldera” sector (Fig. 5).

For a better evaluation of the vulnerability and respective loss (independently of the exposure), the disaggregated losses for each building typology have been normalized by the respective total economic value, as illustrated in Fig. 13b. It is evident that the loss ratios of the most vulnerable typologies, i.e., simple stone structures and pre-code RC buildings, present the highest total loss ratios. Interestingly, the masonry brick vaulted structures (M7) have a relatively low contribution to loss, thanks to their moderate typological vulnerability, no irregularities and their location at the eastern part of the town that presents lower soil amplification.

6 Discussion and Conclusion

Seismic risk is investigated for Fira town, capital of Santorini Island, by combining (a) simulated earthquake ground motions due to a close M5.6 scenario earthquake, (b) macroseismic structural vulnerability concluded via a detailed in situ investigation and (c) site conditions by implementing ambient noise HVSR.

The most vulnerable part of Fira is found to be the old “caldera” sector of the town due to numerous structural interventions of older masonry building preexisting to the disastrous earthquake of 1956. This part of the town exhibits the highest amplification and consequently PGA values, lying though within the limits of the modern seismic design prescriptions of nominal acceleration of 0.24 g for Santorini (Zone II of the seismic code; EAK 2004).

The outcome risk assessment model, constrained on a building block scale, is summarized as: 55% of the surveyed building stock is expected to exhibit no damage, 29% slight damage and 16% is predicted to present moderate-to-heavy damage. For the more vulnerable western “caldera sector,” the damage distribution is as follows: 18% no

damage, 47% slight damage and 35% moderate-to-heavy damage. Taking into account the topography, the urban planning and the high rate of tourism of the area, the latter damage ratios are considered significant.

The monetary loss impact of the studied seismic scenario is estimated about 4 million euros. Although the direct loss estimates may be relatively low with respect to Santorini's wealth, one should account also for eventual indirect losses related to business interruption and/or long-term impact to the tourism, thus vertically increasing the cost of the earthquake.

Two types of uncertainties are recognized to be involved in the process, epistemic and aleatory. Epistemic uncertainties are related to limitations of the HCSR approach, which has proven to underestimate site amplifications (e.g., Rodríguez and Midorikawa 2003). For their treatment, real local earthquake recordings at the same positions with the microtremor measurements are required, which is unfeasible in the frame of the current campaign. Aleatory uncertainties can be due to the quality of the ambient noise measurements and are intrinsically related to transients from human activities.

As far as the uncertainties of the exposure and vulnerability model are concerned, they are mainly described as epistemic, related to (a) the classification of the building stock to a building typology and (b) the assignment of typological seismic performance to each class:

- a. Uncertainties related to the assignment of the building stock to building typologies and to its accurate geometry may be attributed to the difficult accessibility of the urban tissue and/or to inaccurate building footprints captured from satellite images of a highly inclined area. Engineering judgment is believed to have contributed to reducing this type of uncertainties.
- b. Regarding the seismic performance of each typology, the assumed vulnerability indices, derived from statistical and empirical implementation of seismic responses of European buildings, may not necessarily be optimal for the target building stock. The fuzzy set theory and the discrete beta distribution of the mean damage grade though tackle the vagueness problem of the qualitative definitions of the Damage Probability Matrices implemented in EMS-98. Thus, bounds of both the vulnerability index and the assessed DG are provided within the possibility and plausibility range, which manages to limit the uncertainties (Barbat et al. 2008). Uncertainties of this type are considered to be within the range of the ones established by the applied LM1 method.

Since a scope of this study is to be also exploitable by the civil protection authorities, deterministic results are represented only by the most probable values. Sensitivity and parametric analysis by implementation of a logic tree scheme (e.g., Michel et al. 2017) is a future task to allow for the combination of different nodes with variable weights within the risk model.

Thereafter, considering the complex hazardous sources threatening the integrity of the island, it is suggested that secondary seismic effects such as slope instability, rock falling, tsunamis or tephra fallout should be taken into consideration into a future multi-hazard analysis regarding a possible extreme scenario, leading to a holistic risk assessment. Moreover, given the uniqueness of the traditional architecture of Santorini, which is not standardized in macroseismic scales (e.g., EMS-98), further study is needed regarding the seismic response of the local typologies, as well as update of the consequence models. To this direction, building-to-soil spectral ratios are recommended at a future stage to account for soil–structure interaction effects. Furthermore, probabilistic analysis accounting for the latest findings on the Aegean's faults (Papadimitriou et al. 2018) and their recurrence period can lead to scientifically based annual loss estimates.

Quantification of indirect losses, such as declines on revenue due to disruption of the society's activity, is essential for Santorini, given the potential impact of earthquakes on tourism business, and, thus, a risk assessment in refined economic terms is recommended. Other parameters, such as the seasonal variation of the population that jeopardizes the socioeconomic vulnerability, would contribute immensely to the establishment of contingency plans toward the community's preparedness and resilience.

Acknowledgements The study has been realized in the framework of the project RASOR (Rapid Analysis and Spatialisation of Risk), funded by the European Union's Seventh Framework Program for research, technological development and demonstration under Grant Agreement No. 606888. The exposure model of Fira has been implemented in the RASOR platform (<http://www.rasor-project.eu/rasor-case-studies-santorini/>; <http://www.rasor.eu/rasor/>). The authors wish to deeply thank K. Makropoulos, G. Papadopoulos, N. Zorzos, P. Bozineki-Didoni, P. Pelekanos, A. Pomonis for discussions, S. Mourloukos for field work and C. Tsimi for helping in the spatial data analysis. We are indebted to the staff of the Technical Services department of the Fira municipality for helping us in the field. We acknowledge support by the project "HELPOS - Hellenic System for Lithosphere Monitoring" (MIS 5002697).

References

- Barbat AH, Lagomarsino S, Pujades LG (2008) Vulnerability assessment of dwelling buildings, Chapter 6. In: Oliveira CS, Roca A, Goula X (eds) *Assessing and managing earthquake risk*. Springer, Berlin, pp 115–134
- Beresnev IA, Atkinson GM (1998) Stochastic finite-fault modeling of ground motions from the 1994 Northridge, California earthquake. I. Validation on rock sites. *BSSA* 88:1392–1401
- Beriatos E (2008) Uncontrolled urbanization, tourism development and landscape transformation in Greece. 44th ISOCARP Congress, Dalian, China
- Biass S, Bonadonna C, di Traglia F, Pistolesi M, Rosi M, Lestuzzi P (2016a) Probabilistic evaluation of the physical impact of future tephra fallout events for the Island of Vulcano, Italy. *Bull Vulcanol* 78:37. <https://doi.org/10.1007/s00445-016-1028-1>
- Biass S, Falcone JL, Bonadonna C, Di Traglia F, Pistolesi M, Rosi M, Lestuzzi P (2016b) Great balls of fire: a probabilistic approach to quantify the hazard related to ballistics—A case study at La Fossa volcano, Vulcano Island, Italy. *J Vulcanol Geotherm Res* 325:1–14
- Boore DM (1983) Stochastic simulation of high-frequency ground motions based on seismological models of the radiated spectra. *BSSA* 73:1865–1894
- Boore DM (2009) Comparing stochastic point-source and finite-source ground-motion simulations: SMSIM and EXSIM. *Bull Seismol Soc Am* 99(6):3202–3216
- Bozineki-Didoni P (1999) Preservation and development of traditional settlements in Greece. The GNTO programme (1975–1995). The example of Oia-Santorini (personal communication)
- Brune JN (1970) Tectonic stress and spectra of seismic shear waves from earthquakes. *J Geoph Res* 75:4997–5009
- Brüstle A, Friederich W, Meier T, Gross C (2014) Focal mechanism and depth of the 1956 Amorgos twin earthquakes from waveform matching of analogue seismograms. *Solid Earth* 5:1027–1044
- Chouliaras G, Drakatos G, Makropoulos K, Melis NS (2012) Recent seismicity detection increase in the Santorini volcanic island complex. *Nat Hazards Earth Syst Sci* 12:859–866
- Dekavallas K (2013) Earthquake resistant construction of Santorini 1956–1960. *Lect Archit Dep NTUA* 21(03):2013 (in Greek)
- Druitt TH, Edwards L, Mellors RM, Pyle DM, Sparks RSJ, Lanphere M, Davies M, Barriero B (1999). Santorini Volcano, *Geol Soc London Mem* 19
- EAK (2004) Greek Seismic Code, with additional articles. Earthquake Planning and Protection Organization, Athens
- Feuillet N (2013) The 2011–2012 unrest at Santorini rift: stress interaction between active faulting and volcanism. *Geophys Res Lett* 40:3532–3537
- Ganas A, Oikonomou IA, Tsimi C (2013) NOAfaults: a digital database for active faults in Greece, Bulletin of the Geological Society of Greece. In: *Proceedings of the 13th international congress*, Chania, Sept. 2013, vol XLVII. <https://doi.org/10.12681/bgsg.11079>
- GeoMappApp database. Available online at: <http://www.geomappapp.org/>

- Giovinazzi S, Lagomarsino S (2004) A macroseismic method for the vulnerability assessment of buildings. In: Proceedings of the 13th World Conference on Earthquake Engineering 896, Vancouver
- Goretti A, Di Pasquale G (2004) Building inspection and damage data for the 2002 Molise, Italy. *Earthq Spectra* 20(1):167–190
- Global Centroid Moment Tensor Project (GCMT). Available online at: <http://www.globalcmt.org>
- Grünthal G (ed) (1998) European Macroseismic Scale 1998 (EMS-98). Cahiers du Centre Européen de Géodynamique et de Séismologie 15, Centre Européen de Géodynamique et de Séismologie, Luxembourg
- Grünthal G, Wahlstrom R, Stromeyer D (2013) The SHARE European Earthquake Catalogue (SHEEC) for the time period 1900–2006 and its comparison to the European-Mediterranean Earthquake Catalogue (EMEC). *J Seismolog* 17:1339–1344
- Hatzidimitriou P, Papazachos C, Kiratzi A, Theodulidis N (1993) Estimation of attenuation structure and local earthquake magnitude based on acceleration records in Greece. *Tectonophysics* 217:243–253
- Joyner WB, Boore DM (1988) Measurement, characterization, and prediction of strong ground motion. In: *Earthquake engineering and soil dynamics II—Recent advances in ground-motion evaluation: proceedings of the specialty conference GTDiv/ASCE, Park City, Utah*, pp 43–102
- Kahle HG, Straub C, Reilinger R, McClusky S, King R, Hurst K, Veis G, Kastens K, Cross P (1998) The strain rate fields in the eastern Mediterranean region, estimated by repeated GPS measurements. *Tectonophysics* 294:237–252
- Kappos A, Panagopoulos G, Panagiotopoulos C, Penelis G (2006) A hybrid method for the vulnerability assessment of R/C and URM buildings. *Bull Earthquake Eng* 4:391–413
- Kappos A, Panagopoulos G, Penelis G (2008) Development of a seismic damage and loss scenario for contemporary and historical buildings in Thessaloniki, Greece. *Soil Dyn Earthq Eng* 28(10–11):836–850
- Kassaras I, Kalantoni D, Benetatos C, Kaviris G, Michalaki K, Sakellariou N, Makropoulos K (2015) Seismic damage scenarios in Lefkas old town (W. Greece). *Bulletin of Earthquake Engineering*. <https://doi.org/10.1007/s10518-015-9789-z>
- Kaviris G, Papadimitriou P, Kravvariti PH, Kapetanidis V, Karakonstantis A, Voulgaris N, Makropoulos K (2015) A detailed seismic anisotropy study during the 2011–2012 unrest period in the Santorini Volcanic Complex. *Phys Earth Planet Inter* 238:51–88
- Kohno K, Ohmachi T (1998) Ground-motion characteristics estimated from spectral ratio between horizontal and vertical components of microtremor. *BSSA* 88(1):228–241
- Kolaitis A, Papadimitriou P, Kassaras I, Makropoulos K (2007) Seismic observations with broadband instruments at Santorini volcano. *Bull Geol Soc Greece XXXVII*:1150–1161
- Ktenidou OJ, Gélis C, Bonilla LF (2015) A study on the variability of kappa (κ) in a borehole: implications of the computation process. *BSSA*. <https://doi.org/10.1785/0120120093>
- Makropoulos K, Kaviris G, Kouskouna V (2012) An updated and extended earthquake catalogue for Greece and adjacent areas since 1900. *Nat Hazards Earth Syst Sci* 12:1425–1430
- Margaris BN, Boore DM (1998) Determination of $\Delta\sigma$ and ω^2 from response spectra of large earthquakes in Greece. *BSSA* 88(1):170–182
- Michel C, Fäh D, Lestuzzi P, Hannewald P, Husen S (2017) Probabilistic mechanics-based loss scenarios for school buildings in Basel. *Bull Earthq Eng* 15(4):1471–1496. <https://doi.org/10.1007/s10518-016-0025-2>
- Milutinovic Z, Trendafiloski G (2003) An advanced approach to earthquake risk scenarios with applications to different European towns. Report WP4: vulnerability of current buildings, Risk-UE. European Commission, Brussels. https://doi.org/10.1007/978-1-4020-3608-8_23
- Musson RMW, Grünthal G, Stucchi M (2010) The comparison of macroseismic intensity scales. *J Seismol* 14:413–428
- Nakamura Y (1989) A method for dynamic characteristics estimation of subsurface using microtremor on the ground surface. *QR Railw Tech Res Inst* 30:25–33
- New Greek Seismic Code (NEAK) (1994) Earthquake Planning and Protection Organization, Athens, Greece
- Newhall CG (2000) Volcano warnings. In: Sigurdsson H, Houghton BF, Ballard RD (eds) *Encyclopaedia of volcanoes*. Academic Press, San Diego, pp 1185–1197
- Newman AV, Stiros S, Feng L, Moschas F, Saltogianni V, Jiang Y, Papazachos C, Panagiotopoulos D, Karagianni E, Vamvakaris D (2012) Recent geotectonic unrest at Santorini Caldera, Greece. *Geophys Res Lett*. <https://doi.org/10.1029/2012GL051286>
- Nomikou P, Druitt TH, Hübscher C, Mather TA, Paulatto M, Kalnins LM, Kelfoun K, Papanikolaou D, Bejelou K, Lampridou D, Pyle DM, Carey S, Watts AB, Weiß B, Parks MM (2016) Post-eruptive

- flooding of Santorini caldera and implications for tsunami generation. *Nat Commun.* <https://doi.org/10.1038/ncomms13332>
- Nomikou P, Hübscher C, Papanikolaou D, Farangitakis GP, Ruhnau M, Lampridou D (2017) Expanding extension, subsidence and lateral segmentation within the Santorini—Amorgos basins during Quaternary: Implications for the 1956 Amorgos events, central—south Aegean Sea, Greece. *Tectonophysics* 722:138–153
- Okal EA, Synolakis CE, Uslu B, Kalligeris N, Voukouvalas E (2009) The 1956 earthquake and tsunami in Amorgos, Greece. *Geophys J Int* 178:1533–1554
- Papadimitriou P, Kapetanidis V, Karakonstantis A, Kaviris G, Voulgaris N, Makropoulos K (2015) The Santorini Volcanic Complex: a detailed multi-parameter seismological approach with emphasis on the 2011–2012 unrest period. *J Geodyn* 8:32–57. <https://doi.org/10.1016/j.jog.2014.12.004>
- Papadimitriou P, Kassaras I, Kaviris G, Tselentis GA, Voulgaris N, Lekkas E, Chouliaras G, Evangelidis Ch, Pavlou K, Kapetanidis V, Karakonstantis A, Kazantzidou-Firtinidou D, Fountoulakis I, Millas Ch, Spingos I, Aspiotis Th, Mousoulidou A, Em Skourtsos, Antoniou V, Em Andreadakis, Sp Mavroulis, Kleanthi M (2018) The 12th June 2017 Mw = 6.3 Lesbos earthquake from detailed seismological observations. *J Geodyn* 115:23–42
- Papadopoulos GA, Pavlides SB (1992) The large 1956 earthquake in the South Aegean: Macroseismic field configuration, faulting, and neotectonics of Amorgos Island. *Earth Planet Sci Lett* 113:383–396
- Papazachos BC, Comninakis PE (1971) Geophysical and tectonic features of the Aegean Arc. *JGR* 76(35):8517–8533
- Papazachos BC, Panagiotopoulos D (1993) Normal faults associated with volcanic activity and deep rupture zones in the southern Aegean volcanic arc. *Tectonophysics* 220:301–308
- Papazachos B, Papazachou C (2003) The earthquakes of Greece, 3rd edn. Ziti Publications, Thessaloniki
- Papoutsis I, Papanikolaou M, Floyd K, Ji H, Kontoes C, Paradissis D, Zacharis V (2013) Mapping inflation at Santorini volcano, Greece, using GPS and InSAR. *Geophys Res Lett* 40:267–272. <https://doi.org/10.1029/2012GL054137>
- Petersen ADJ (2004) A geological and petrological study of the dikes in the Megalo Vouno volcano complex, Santorini. Ph.D. Thesis, Copenhagen University
- Rodríguez VHS, Midorikawa S (2003) Comparison of spectral ratio techniques for estimation of site effects using microtremor data and earthquake motions recorded at the surface and in boreholes. *Earthq Eng Struct Dyn* 32:1691–1714
- SERTIT (SErvice Régional de Traitement d'Image et de Télédétection) http://sertit.u-strasbg.fr/index_en.htm
- SESAME (2005) Guidelines for the implementation of the H/V spectral ratio technique on ambient vibrations—measurements, processing and interpretations. SESAME European research project EVG1-CT-2000–00026, deliverable D23.12
- Stasinopoulos T (2002) Santorini “The blue drinkable volcano”. Notes for 1st year of Department of Architecture, National Technical University of Athens, Greece
- Statistical Authority of Greece (EL.STAT.) (2011) Buildings census. Available online at: <http://www.statistics.gr/el/2011-census-pop-hous>
- Tselentis G, Danciu L (2008) Empirical relationships between modified Mercalli intensity and engineering ground-motion parameters in Greece. *BSSA* 98(4):1863–1875
- Vallianatos F, Michas G, Papadakis G, Tzanis A (2013) Evidence of nonextensivity in the seismicity observed during the 2011–2012 unrest at the Santorini Volcanic Complex, Greece. *Nat Hazards Earth Syst Sci* 13:177–185
- Wang J (1993) Seismic design of tunnels—a simple state-of-the-art design approach. Parsons Brinckerhoff, New York
- Wells DL, Coppersmith KJ (1994) New empirical relationships among magnitude, rupture length, rupture width, rupture area, and surface displacement. *BSSA* 84(4):974–1002